Measurements of micro-turbulence in high beta and high density regimes of LHD and comparison with resistive g-mode scaling

Clive MICHAEL[1)], Kenji TANAKA[1)], Leonid VYACHESLAVOV[2)], Andrei SANIN[2)], Tsuyoshi AKIYAMA[1)], Yoshiro NARUSHIMA[1)], Kiyomasa WATANABE[1)], Hisamichi FUNABA[1)], Sadayoshi MURAKAMI[3)] Katsumi IDA[1)], Mikiro YOSHINUMA[1)], Ryuichi SAKAMOTO[1)], Kazuo KAWAHATA[1)], and Shigeki OKAJIMA[4)]

[1)]*National Institute of Fusion Science, Toki 509-0293, Japan* [2)] *Budker Institute for Nuclear Physics, Novisibirsk, Russia* [3)] *Department of Nuclear Engineering, Kyoto Univ., Kyoto 606-8501, Japan* [4)] *Chubu University, Kasugai, Japan*

November 26, 2007

Density fluctuations are analyzed in high volume average beta and high core density discharges in the Large Helical Device (LHD) using a 2D phase contrast imaging system and far infra-red interferometer. Though both these regimes share similarly high beta gradients, the physical origin of the fluctuations appears to be different. In high volume average beta plasmas, both large and ion-gyro scale density fluctuation levels are compared with the growth rate of resistive interchange modes and a clear correlation is found most particularly in the edge as expected due to having the strongest magnetic hill in this region. In high core density plasmas with internal diffusion barrier, resistive interchange is not a candidate for fluctuations near the barrier because magnetic well exists there. However, fluctuations near the core have a bursty character in time and are destabilized when the temperature profile is transiently hollow immediately after pellet injection and are quiescent and much reduced when it becomes peaked, consistent with a slab ion temperature gradient mode. In configurations with outward shifted magnetic axis, where core plasma pressure and density are greater, fluctuation bursts occur less frequently suggesting anomalous transport is lower.

Keywords: high beta, density fluctuation, phase contrast imaging, MHD, resistive interchange, super dense core regime, ion temperature gradient turbulence

1 Introduction

The Large Helical Device (LHD) has set many impressive results with respect to high performance plasma operation, including operation at low field ($B \sim 0.425$T), high volume average beta (up to 5%) [1], as well as at high field ($B > 2$T), high central beta with high central density produced through an internal diffusion barrier (IDB) [2]. Such high performance regimes are invaluable for fusion reactor operation; high volume average beta for reduction of magnetic field requirement, and high central density operation for production of another possible route to fusion through low temperature, high density operation. It is essential to gain an understanding of limiting factors influencing the performance of these plasmas for a route to a fusion reactor, in particular energy transport, which degrades the performance (such as beta gradient, density gradient, etc) either in a soft manner (gradually increasing with performance) or a hard manner (increasing suddenly above a performance threshold). Transport studies have been carried out on these regimes [3], it is mostly found that transport exceeds the neoclassical level significantly and that it is dominated by fluctuation-driven processes. Moreover, high density operation is not well studied yet. Therefore this study focuses on fluctuation behavior in high performance discharges from measurements based on 2D CO2 laser phase contrast imaging and FIR interferometer, and the role that these fluctuations play on transport.

These two regimes are studied separately, and some attempt is made to unify the results of these regimes, given that they both share high beta (pressure) gradients, which are free energy sources for fluctuations. However, the important processes in each regime appear to be different. In high volume average beta, the main confinement degradation comes from the edge where resistive interchange (or g mode) turbulence appears to be excited as a result of the magnetic hill common to Stellarators and RFPs. In the high core density discharges [4], resistive g is not a candidate for turbulence around the internal diffusion barrier because magnetic well exists in the inner region. In this case it appears that the opposite sign of density and temperature profiles, produced transiently after pellet injection, appears to strongly drive unstable modes in a burst like fashion characteristic of a very hard critical threshold. This is characteristic of a slab ITG mode instability; though other MHD effects such as a ballooning mode may play a role. It appears that outward shifted configurations have less hollow temperature profiles resulting in lower fluctuation level therefore achieving higher central pressure.

This paper is organized as follows. The density fluctuation diagnostic systems are first discussed in Sec 2; in-

author's e-mail: clive@nifs.ac.jp

cluding the technique for spatial localization from line-integrated measurements. In Sec. 3, we introduce measurements in high volume average beta discharges, including theory, experiments and results of dependence of fluctuation (of both large scale and ion gyro-scale) level and position on beta, as well as a comparison of fluctuation characteristics with thermal conductivity obtained from power balance. In Sec. 4, we present the dynamical evolution of core turbulence level in dense core discharges for plasmas in configurations with vacuum magnetic axis position $R_{ax} = 3.65\text{m}, 3.75\text{m}$, and compare with differences of pressure rise. Finally, in Sec. 5, we summarize and compare these regimes.

2 Density fluctuation measurements with CO2 laser phase contrast imaging and FIR interferometer

For density fluctuation measurements we use the CO2 laser 2D phase contrast imaging diagnostic for diagnosis of ion gyro-scale fluctuations (with $1 < k < 10\text{cm}^{-1}$), and the FIR interferometer [5] for diagnostic large scale fluctuations (with $k < 1\text{cm}^{-1}$). Phase counters of the FIR have sufficient precision (1/60 fringe) and bandwidth ($f < 50$kHz) to diagnose fluctuations at high beta, though at low beta, the fluctuation level is comparable to the noise. Note that the PCI diagnostic does not admit $k = 0$ components because of its optical arrangement, while the FIR interferometer does. Both the PCI and FIR systems only directly measure the line integrated density fluctuation amplitude, rather than the local value. However, with the 2D PCI diagnostic, some moderate spatial resolution is possible as described below. Routinely the fluctuation components near the edge are much stronger than any core components, so for diagnosis of edge resistive g modes, line-integral values are sufficient, but for detailed analysis, and for analysis of turbulence near the core of high core density discharges, a proper analysis to resolve fluctuations along the line of sight is necessary to analyze changes in core fluctuations as distinct from edge fluctuations.

The 2D phase contrast imaging diagnostic system on LHD employs a 2D imaging principle to split the line-integrated fluctuation signal into contributions from different layers along the line of sight, according to the "magnetic shear" principle [6, 7, 8]. The sightline is vertical passing at $R = 3.603$m, so penetrates from the edge to the core, depending on the magnetic axis position of the plasma (R_{ax}), implying core and edge fluctuation components (from both top and bottom) can be separated. The system cannot, however, fundamentally recover the local fluctuation amplitude because of line-integration effects unless the spectrum is isotropic, which it generally is not [**?**]. The line-integrated $\tilde{N}$ signal is split into contributions along the line of sight and is related to the local amplitude $\tilde{n}$ according to $\tilde{N}^2(\rho) = \tilde{n}^2(\rho) l_z l_{res}$, where l_z represents the ratio of fluctuation power propagating exactly perpendicular to the probing beam to the total fluctuation power, and l_{res} is an instrumental resolution which is increases with measured fluctuation wavelength. For typically measurements, the peak wavelength is such that the instrumental width is around half a radius, or less near the edge because the average wavelength is generally smaller than in the core.

3 High volume average beta

For high volume average beta plasmas, turbulent transport induced by resistive interchange modes excited, driven by beta gradient in the magnetic hill region in the edge is expected to be a limiting mechanism on the attainable plasma beta in helical devices. In LHD, these modes have been shown to have a "soft" character since their occurrence does not produce a catastrophic effect on plasma operation and since plasma operation has been extended well beyond the Mercier instability boundaries [9]. This is in contrast to pressure (beta) driven instabilites in the edge of Tokamak devices, such as ELMS, which grow very quickly beyond the instability threshold producing a sudden crash. Though the physical mechanism is different, such as a peeling-balooing modes, since the Tokamak does not have magnetic hill because the toroidal current is internal to the plasma. Low order mode numbers are routinely identified and have been compared successfully to predictions of resistive interchange modes [10]. However, theoretically, resistive interchange can be excited up to high order mode numbers, up to the dissipative gyro-scale. Non-adiabatic response due to resistive effects produces an anomalous flux. This is in contrast to a turbulent transport induced by drift wave type instabilities (such as ion temperature gradient (ITG) and trapped electron mode (TEM)) whose drive mechanisms do not depend so directly on beta, rather on functions of normalized density (L_n^{-1}) and temperature (L_T^{-1}) gradients such as $\eta = L_T^{-1}/L_n^{-1}$ (although they are known to be stabilized at higher beta [11]). Because drift and resistive interchange instabilities coexist in the same spatial scale, distinction between them becomes difficult. However, they can be distinguished possibly in (1) coherence with magnetic fluctuations, since ITG/TEM are electro-static, while resistive-g has a magnetic component. In reality, however this may be difficult to detect for ion gyro-scale fluctuations, since magnetic probes external to the plasma are most sensitive to large scale fluctuations and the non-locality of magnetic probe measurements would tend to reduce the coherence of small scale fluctuations, and (2) phase velocity; drift waves propagate poloidally at around the drift velocity plus ExB velocity while resistive interchange turbulence propagates at only the ExB velocity [12].

Previous work on LHD [13] has looked at the role of resistive interchange turbulence and its relationship to the

electron heat transport coefficient, and it was shown that at high beta, a transport increases more strongly with beta than predicted by a simple gyro-Bohm type model (incorporating drift wave instabilities); and that a model describing resistive interchange turbulence accurately reproduced the beta tendency of electron heat conductivity. This established (1) the role of high beta/ resistive g on energy transport. Here, however, we plan to show the other possible links, (2) role of high beta on fluctuations and (3) role of fluctuations on energy transport. This is the first such work of a comparison of density fluctuations and energy transport; previously particle transport coefficients were compared with the fluctuation level in low beta high field discharges [14].

3.1 Theory of resistive interchange turbulence

A simple analytic theory verified by numerical simulation was developed by [15, 16, 17]. The growth rate is given as:

$$\gamma = S^{-1/3}\left(\nabla\beta\frac{R_0^2\kappa_n}{2}m\frac{2\pi d\rho}{d\iota}\right)^{2/3}\tau_{hp}^{-1} \quad (1)$$

where, the magnetic Reynolds number $S = \tau_R/\tau_{hp} \propto T^{3/2}n^{-1/2}$, the resistive skin time $\tau_R = r^2\mu_0/\eta$, and the poloidal Alfvén time $\tau_{hp} = R_0\sqrt{\mu_0 m_i n}/B$, with $\eta \propto T^{3/2}n^0$ being the Spitzer resistivity. Therefore, the scaling of the growth rate is not simply given by $\beta = n_eT_e/B^2$, it is given by:

$$\gamma \propto n_e^{1/6}(n_eT_e)^{1/6}B^{-2/3}\kappa_n^{2/3}L_p^{-2/3} \quad (2)$$

Under this theory, the thermal conductivity is:

$$\chi = \gamma W^2, \quad (3)$$

where W is the radial width of the mode [16]. This theory does not clearly guide which is quantity is relevant to compare with density fluctuation level. On one hand, Eq. (3) is derived from mixing length theory, for which $\tilde{n}/n = \lambda/L_n$ where λ is the wavelength of the fluctuation and L_n is the density scale length, therefore being independent of growth rate γ. The γ dependence in Eq. (3) comes from the associated velocity fluctuation amplitude. There are many criticisms to the use of linear growth rates for assessing fluctuation level when another physical process is important for saturation. However, in one study, non-linear and linear simulations have been shown to agree [18]. Therefore, for this case, we compare fluctuation levels $\tilde{n}/n$ with γ, however the obtained increasing trend goes against simple mixing length theory.

3.2 Fluctuation measurements and consistency with resistive g

For this study, density, temperature and magnetic field strength were systematically varied in a series of discharges. At certain times during the flat-top of each discharge when the plasma was at equilibrium, fluctuation and

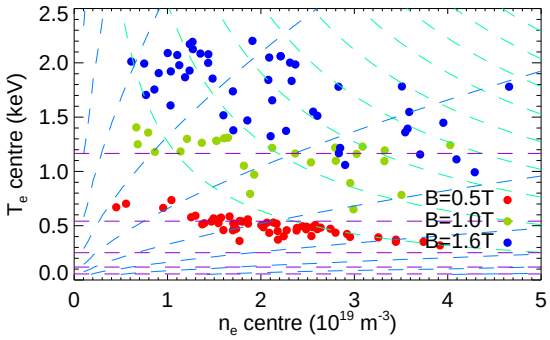

Fig. 1 Density, temperature and magnetic field strengths covered over in the parameter scans, together with contours of β, ν_{ei} and Larmor radius.

parameter profiles were stored in a small database to be analyzed. The range of central densities and electron temperatures, and magnetic field strengths spanned are shown in Fig. (1), together with lines of constant β, ν_{ei} (related to magnetic Reynolds number S), and gyro-radius. It can be seen that the temperature does not change strongly with density. The volume average $\beta_{\rm vol}$ reached only up to 3% in these discharges as the helical pitch configuration parameter was $\gamma = 1.25$ rather than $\gamma \sim 1.20$ at which the recent very high beta shots were obtained [1]. The value $\beta_{\rm vol}$ was calculated from measured density and electron temperature values, applying a single correction factor for all discharges to match the average diamagnetic β.

The $\beta_{\rm vol}$ dependence of the line integrated fluctuation levels from the FIR and PCI systems as described in Sec. (2) are plotted in Fig. (2). It is clear that for both systems, there is a strong increasing trend of fluctuation level with β. The increase with $\beta_{\rm vol}$ appears to be most significant for $\beta_{\rm vol} > 1\%$, consistent with the findings that $\chi_{exp}/\chi_{gmod} = 1$ for $\beta_{\rm vol} > 1\%$ in [13], where χ_{exp} is the experimentally derived thermal conductivity and χ_{gmod} is the resistive g mode growth conductivity as in Eq. (3). For the 2D PCI (with $k > 1{\rm cm}^{-1}$), the fluctuation level appears to double roughly as beta goes from $\sim$ 0.3% to 3%, while for the FIR, which measures $k < 1{\rm cm}^{-1}$, the increase is much larger. This may be attributed to the fact that resistive interchange turbulence can drive both large scale and ion gyro-scale fluctuations, and has a strong beta dependence, while the level of electrostatic drift wave turbulence (ITG/TEM), which does not depend so explicitly on beta, is strong at the ion gyro-scale but non-existent at large scales. In both diagnostics there also appears to be a large scatter at high β. This may be due to (1) the loss of detail due to line-integration effects, and (2) the resistive g mode growth rate has additional dependence than simply $\beta_{\rm vol}$. The motivates us to look more in detail at the comparison of the fluctuation level with the resistive g mode growth rate scaling formula as written in Eq. (2).

A local analysis is performed on one shot from the

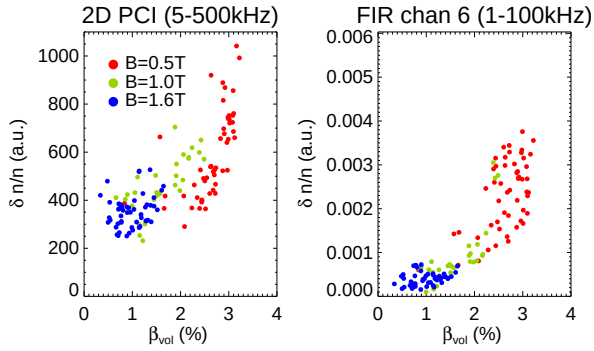

Fig. 2 $\beta_{\rm vol}$ dependence of line integrated fluctuation level for both (a) ion gyro scale structures with $k > 1\text{cm}^{-1}$ from 2D PCI, and (b) large scale structures with $k < 1\text{cm}^{-1}$ from the FIR interferometer.

database at $\beta_{\rm vol} = 2.5\%$ considering profiles of density, temperature and pressure, density fluctuation amplitude and normal curvature κ_n, as plotted in Fig. (3). Profiles of fluctuation amplitude both above and below the mid-plane are shown, considering the Shafranov shift as determined from Thomson scattering. The mismatch of these two profiles may be attributable to either (1) because different directional wave-vector components are measured on the top compared with the bottom, or because (2) fluctuation structure is not symmetric on a flux surface, possibly due to ballooning structure. The spatial resolution is around $\Delta\rho = 0.2$ at the edge and around $\Delta\rho = 0.5$ towards $\rho = 0.3$, because the average k is higher towards the edge and since $\Delta\rho \propto 1/k$. The strongest peak appears around $\rho = 1.05$, and appears to correspond to a peak in the pressure gradient profile, plotted in Fig. (3c), demonstrating that pressure gradient may be the free energy source at the edge. However, the normal curvature is positive only outside $\rho = 0.75$ so the the fluctuation power inside this radius must be driven by a different mechanism other than resistive interchange.

Taking the component at $\rho = 0.9$, we compare the local $\tilde{n}/n$ with the local g-mode growth rate in Fig (4). It can be seen that there is a much clearer relationship than in Fig. (2), particularly at higher γ. The cause of this better agreement is the increased density dependence arising from the S dependence in Eq. (2). This density dependence is highlighted in Fig. (5), where line integrated $\tilde{N}/N$ is compared with both $\langle nT\rangle/B^2 \sim \beta_{\rm vol}$ and $\langle n(nT)\rangle/B^2$ (where $\langle\rangle$ denotes volume averaging). The χ^2 residual of points conforming to a smooth curve is a factor of two better in the case of the stronger density dependence (b). (Note, however that the g-mode growth rate γ_g^6 from Eq. (2) has a B^{-4} scaling as compared with the B^{-2} dependence here.)

The increased density dependence is also highlighted by comparing 2 discharges with similar $\beta_{\rm vol}$, but significantly different density. The profiles of fluctuation level $\tilde{n}/n$, n, T and are compared in Fig. (6). It is clear that

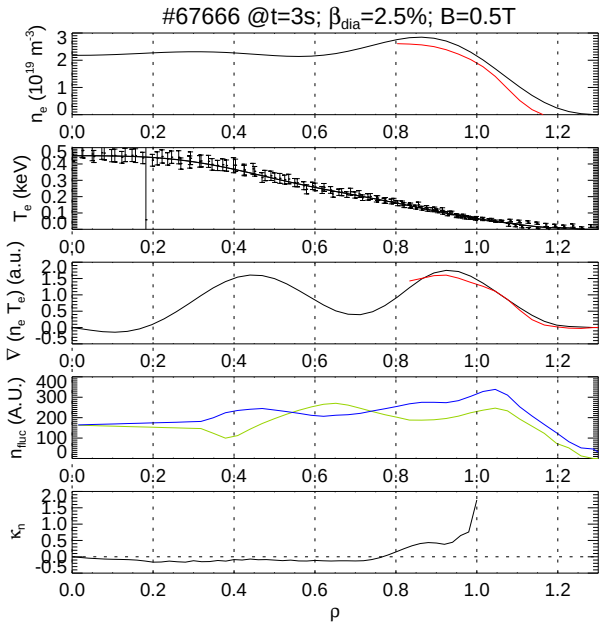

Fig. 3 Comparison of profiles (a) density, (b) temperature, (c) pressure gradient, (d) fluctuation amplitude, and (e) normal curvature κ_n for a shot with $\beta_{\rm vol} = 2.5\%$.

the higher density discharge has about twice the fluctuation level, and is largest between $\rho = 0.8 - 1.0$ where resistive g is located. The scaling of fluctuation level here is clearly attributable to stronger density, despite having similar $\beta_{\rm vol}$.

The position of the strongest fluctuation peak as a function of $\beta_{\rm vol}$ is plotted in Fig. (7), separated out into parts above and below the mid-plane, as discussed before. As $\beta_{\rm vol}$ is increased, the region of magnetic well extends towards the edge, as indicted by the shaded region, meaning that the resistive g peaks must be localized further towards the edge at higher beta. This seems to be consistent with the measured positions, indicated by dots, more particularly for components on the bottom. For components on the top, there appears to be a concentration of peaks

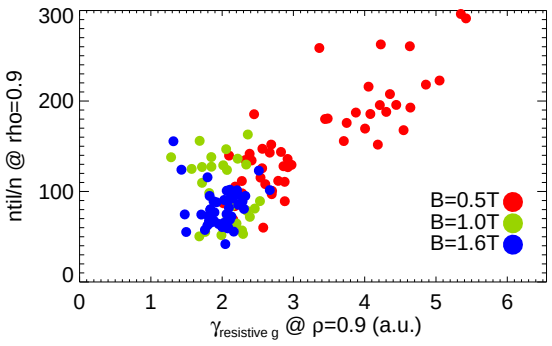

Fig. 4 Comparison of local fluctuation amplitude $\tilde{n}/n$ at $\rho = 0.9$ and resistive g driving growth rate γ_g at the same ρ.

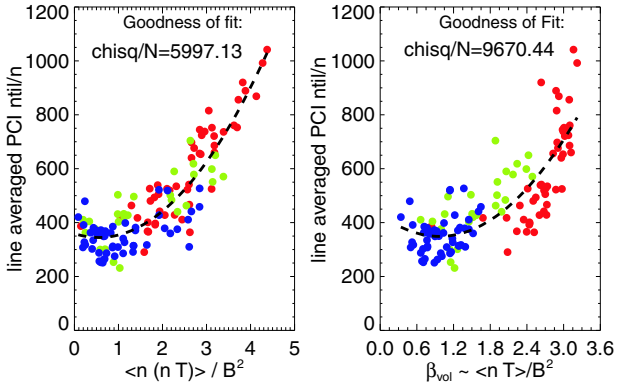

Fig. 5 Dependence of Line integrated fluctuation level from PCI on (a) $\langle n(nT)\rangle/B^2$, and (b) $\beta_{\rm vol}$.

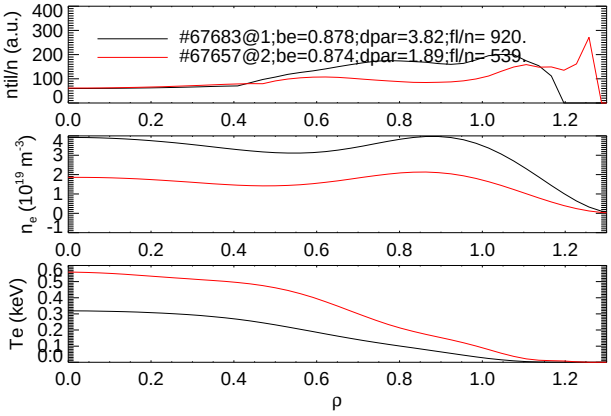

Fig. 6 For shots with similar $\beta_{\rm vol}$, but significantly different density, comparison of profiles of (a) fluctuation level $\tilde{n}/n$, (b) density, (c) temperature.

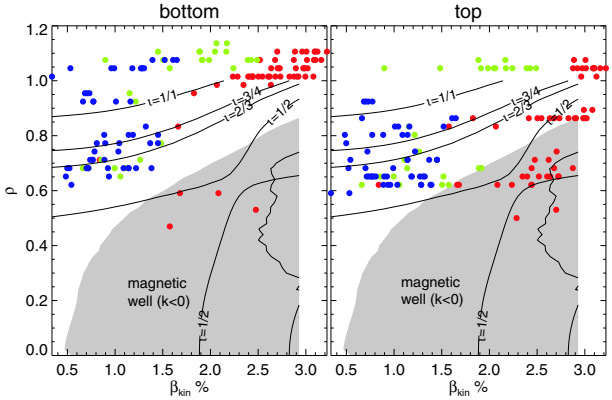

Fig. 7 Position ρ of strongest peak of $\tilde{n}(\rho)$ on (a) bottom and (b) top sides of the midplane, as a function of $\beta_{\rm vol}$, compared with changes in the magnetic structure including well/hill boundary and rational surfaces

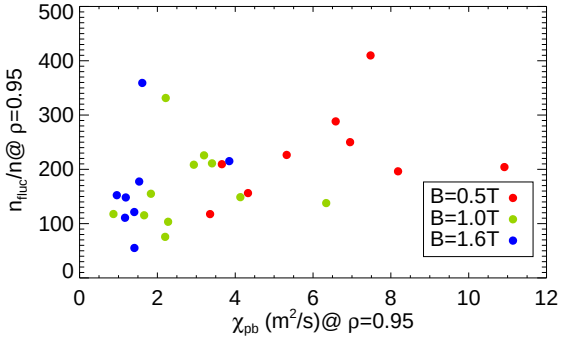

Fig. 8 Comparison of χ with $\tilde{n}/n$ from 2D PCI at $\rho = 0.95$.

around the $\iota = 1/2$ rational surface, approximately where the magnetic shear is close to zero. This type of MHD activity close to rational surfaces has also recently been reported in [19].

In summary, all these results appear to demonstrate the consistency between measured fluctuation amplitudes and positions and the expectation with resistive g mode. The largest discrepancies are from the existence of fluctuations inside the region of magnetic well which may be some drift wave component. Hybridization of resistive g and drift-waves is also possible [17]. This distinction could be more rigourously made on the basis of the difference between the poloidal phase velocity and to the ExB velocity, or the coherence between density and magnetic fluctuations.

3.3 Comparison of fluctuation amplitude with power balance χ at high β

The role of fluctuations on confinement itself is very important to confirm the original assertion that transport is dominated by anomalous processes; and to check that the measured fluctuations are important for confinement, even regardless of the role of what is the driving mechanism of the fluctuations (resistive g or drift wave). For the set of discharges analyzed above, power balance analysis was carried out to determine the "effective" thermal conductivity $\chi = (\chi_e + \chi_i)/2$ as per the procedure described in [13], based on the FIT code [20] which computes the power deposition from NBI by calculating fast particle orbits and their interactions with bulk plasma. The PROCTR code [21] is then used to analyze the diffusivity. For the comparison we choose to compare the edge local fluctuation level with the edge χ ($\rho = 0.95$). The results, for a selected subset of shots in the previous section are plotted in Fig. (8). It is clear that there is is an increasing trend of fluctuation level and conductivity. However, there are significant outliers; these may be due to the fact that turbulence saturates to a level depending on the power input, rather than on the conductivity itself (dependent on gradient), because the gradient steepens to a value such that the heat flux balances the input power in steady state. [*** put this figure in too***].

4 High core density

Recently, pellet-fueled high density plasmas were achieved with central density approaching $10^{21}\mathrm{m}^{-3}$ [2, 4]. These plasmas are characterized by having a high density core with a "diffusion barrier" around mid radius, correlating with the position of zero magnetic shear. Though these plasmas are made at high field ($B > 2$T), the central beta approaches that of the high volume average beta plasmas, and so the beta gradients in the diffusion barrier region are very high; therefore they may have some similar characteristics to high volume average beta plasmas. However, the diffusion barrier is always in the region of magnetic well, meaning that resistive interchange turbulence is not a candidate to explain turbulence.

It has recently been shown [4] that the maximum attainable central density and stored energy increases as the magnetic configuration is changed to move the magnetic axis further outward. For formation of the diffusion barrier, and improved performance at outward shifted configurations, turbulent transport play a significant role. In a separate study [22], the temporal evolution of turbulence (from 2D PCI) and particle particle transport studied after multiple pellet injection with in the configuration with vacuum $R_{ax} = 3.6$m. In this analysis, fluctuation and plasma properties are compared between $R_{ax} = 3.65$m and $R_{ax} = 3.75$m, to confirm whether fluctuation properties are reduced in line with improved confinement. Because the 2D PCI sightline passes around $R = 3.603$m, as the magnetic axis moves outwards, the system is no longer sensitive to core fluctuation properties. In particular, for the highest performance around $R_{ax} = 3.9$m, fluctuations around the diffusion barrier cannot be measured; however, they can be measured sufficiently up to $R_{ax} = 3.75$m for which the sightline penetrates down to $\rho = 0.4$.

The time evolution of the central pressure, computed from Thomson scattering, and fluctuation level $\tilde{n}/n$ at $\rho = 0.4$ are compared for both configurations in Fig. (9). After pellet injection, the temperature is reduced considerably, and the density falls, while the temperature rise so that the pressure rises. It can be seen that at $R_{ax} = 3.75$m, the pressure has risen more quickly and to a higher value than in the case of $R_{ax} = 3.65$m. The fluctuation behavior changes strongly in time after pellet injection. In both configurations, there appears to be strong bursts in time, up to a time when the bursts no longer occur and the fluctuation level is dramatically reduced. However, it is easy to notice that in the $R_{ax} = 3.75$m case, bursts persist over a shorter period of time, and there appears to be a "quiet" period between the bursts meaning that the time average fluctuation level, and hence induced transport, should be smaller. This correlates with the stored energy being higher in this case, so it demonstrates that the reason for the higher pressure may be due to reduced fluctuation level despite stronger density/pressure gradient.

One possible reason for the reduced fluctuation level

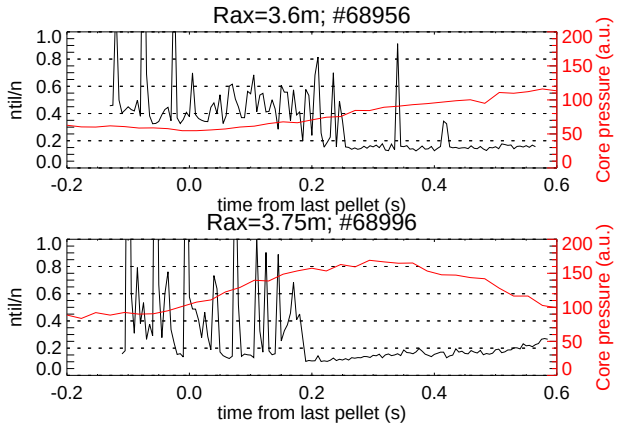

Fig. 9 Comparison of the time evolution of the central pressure, computed from Thomson scattering, and fluctuation level $\tilde{n}/n$ at $\rho = 0.4$ for configurations with (a) $R_{ax} = 3.65$m and (b) $R_{ax} = 3.75$m

when the pressure is higher is due to the difference of the hollowness of the temperature profile, which is produced transiently after pellet injection. Contour plots of the electron temperature profile evolution are shown for both cases in Fig. (10). The temperature profile is more hollow immediately after pellet injection in the inward shifted case ($R_{ax} = 3.65$). For $R_{ax} = 3.65$m, the temperature profile switches from hollow to peaked At $t - t_0 = 0.25$s, around about the same time as the bursts of fluctuations disappear. The same is true for $R_{ax} = 3.75$m, where the profile switches from hollow to peaked and fluctuations disappear at around $t - t_0 = 0.18$s. This indicates that the opposite sign of temperature and density gradient is unstable. Such an instability threshold is characteristic of a slab ITG mode but this does not discount other possible drive mechanisms such as ballooning modes. Because the case of $R_{ax} = 3.75$m has a less hollow temperature profile, it is closer to marginal stability and so fluctuation bursts do not occur so frequently.

The burst-like nature of fluctuations observed in dense core plasmas is similar in nature to ELM activity in the edge of Tokamak devices. In both cases, these occur when the pressure gradient is very high, but in the case here, it seems that pressure gradient does not drive the mode, rather some simple ITG-like mode. The bursts may be due to the profiles being near a marginal stability threshold, and that the instability has a very distinct hard threshold. Such ITG instability thresholds have been demonstrated in Tokamak transport before.

[1] K. Y. Watanabe. Confinement study on the reactor relevant high beta lhd plasmas. In *these proceedings*, (2007).
[2] N. Ohyabu *et al.* Phys Rev Lett **97**, 055002/1 (2006)
[3] K Tanaka *et al.* Nucl Fusion **46**, 110 (2006)
[4] R. Sakamoto these proceedings (2007)
[5] K. Kawahata *et al.* Fusion Eng & Des **34-35**, 393 (1997)
[6] A.L. Sanin *et al.* Rev Sci Instrum **75**, 3439 (2004)

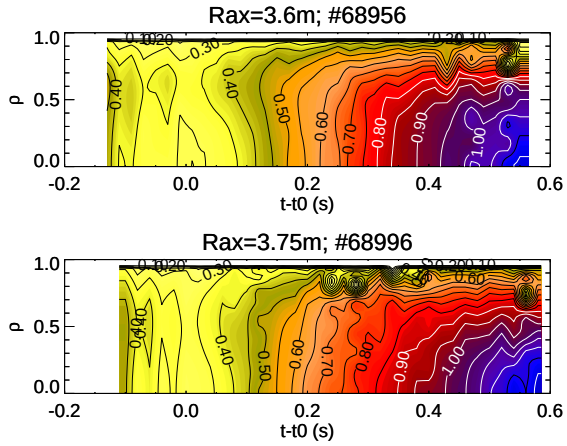

Fig. 10 Contour plots of temporal/spatio evolution of temperature profiles from Thomson scattering (fitted with a polynomial) after pellet injection for configurations with (a) R_{ax} = 3.65m and (b) R_{ax} = 3.75m.

[7] L.N. Vyacheslavov IEEE transactions on plasma science **33**, 464 (2005)
[8] CA Michael *et al.* Rev Sci Instrum **77**, 10E923 (2006)
[9] K. Y. Watanabe *et al.* Nucl Fusion **45**, 1247 (2005)
[10] A. Komori *et al.* Phys Plasmas **12**, 56122 (2005)
[11] P Snyder. Phd thesis, Princeton, (1999).
[12] K. Tanaka *et al.* J Phys Soc JPN **62**, 3092 (1993)
[13] H. Funaba *et al.* Fusion Sci Technol **51**, 129 (2007)
[14] K. Tanaka *et al.* Fusion Sci Technol **51**, 97 (2007)
[15] B. A. Carreras *et al.* Phys Fluids **30**, 1388 (1987)
[16] B. A. Carreras and P. H. Diamond Phys Fluids B **1**, 1011 (1989)
[17] M. Wakatani AIP Conf Proc pages 141 (1997)
[18] T. Dannert and F. Jenko Phys Plasmas **12**, 72309 (2005)
[19] K. Ida *et al.* Phys Rev Lett page submitted (2007)
[20] S. Murakami *et al.* Fusion Technology **27**, 256 (1995)
[21] H Howe ORNL/TM-11521 (1990)
[22] K Tanaka. In *H mode Workshop*, Tsukuba, Japan, (2007).